

Functional Brain-to-Brain Transformation with No Shared Data

Navve Wasserman, Roman Belyi, Roy Urbach, and Michal Irani

The Weizmann Institute of Science

Abstract

Combining Functional MRI (fMRI) data across different subjects and datasets is crucial for many neuroscience tasks. Relying solely on shared anatomy for brain-to-brain mapping is inadequate. Existing functional transformation methods thus depend on shared stimuli across subjects and fMRI datasets, which are often unavailable. In this paper, we propose an approach for *computing functional brain-to-brain transformations without any shared data*, a feat not previously achieved in functional transformations. This presents exciting research prospects for merging and enriching diverse datasets, even when they involve distinct stimuli that were collected using different fMRI machines of varying resolutions (e.g., 3-Tesla and 7-Tesla). Our approach combines brain-to-brain transformation with image-to-fMRI encoders, thus enabling to learn functional transformations on stimuli to which subjects were never exposed. Furthermore, we demonstrate the applicability of our method for *improving image-to-fMRI encoding of subjects scanned on older low-resolution 3T fMRI datasets, by using a new high-resolution 7T fMRI dataset* (scanned on different subjects and different stimuli).

1 Introduction

Functional MRI (fMRI) has emerged as a powerful non-invasive method for measuring human brain activity in real-time, allowing researchers to observe which areas of the brain are involved in different functions and behaviors [1, 2, 3, 4, 5]. However, the time-consuming and expensive data acquisition process of fMRI often leads to limited data availability. Moreover, inter-subject variability in brain structure and functionality poses additional challenges in analyzing fMRI data from multiple subjects, as different individuals may exhibit distinct brain activity patterns even in response to similar stimuli. To address these limitations, functional brain-to-brain transformation has been proposed. Functional brain-to-brain transformation involves learning inter-subject transformations that map the fMRI signals of one subject to the fMRI signals of another. Those transformations allow for the use of data collected from multiple subjects, thereby enriching the available data and enabling comparisons of brain activity across individuals and groups.

While the visual cortex exhibits similarities in topography and organization of functional regions across humans, there are fine-grained functional differences between individuals [6, 7, 8, 9]. This variability poses challenges in comparing and mapping fMRI activation between individuals. As such, traditional anatomical alignment methods [10, 11, 12, 13] have limited functional predictive power across subjects [10, 14, 15, 16]. To address this issue, functional alignment methods have been developed to match the functional behaviors of different individuals by learning relationships between brain activity patterns [14, 15, 17, 18, 19]. There are two main approaches in functional alignment: the first maps subjects into a high-dimensional shared space, with the most well-known method being Hyper-alignment [14, 20, 21, 22], and the second transforms directly between fMRI of two subjects using a conversion model [15]. *However, training these methods requires a large amount of “shared data” namely, fMRI obtained by showing the same stimuli to different subjects. This limits the number of available training examples, and makes it impossible to learn transformations across subjects which have no shared data.* The requirement for shared data thus undermines the ability to combine information from multiple different fMRI datasets, accumulated over the years from a wide variety of visual stimuli from different individuals.

In this paper, we introduce for the first time, an approach for computing functional brain-to-brain transformation without any shared data. Figure 1 formulates the problem setting. Our approach (illustrated in Figure 2), employs “visual encoders”, which are trained individually on subject-specific data, to encode images into subject-specific fMRI. Our method effectively uses visual encoders to predict fMRI of images not seen by a subject. This allows to use also “non-shared data” (which refers to images seen by only one subject), and “external images” (which refers to images not seen by any of the subjects, i.e. arbitrary images without fMRI recordings). To the best of our knowledge, we are the first to employ visual encoders to compute brain-to-brain

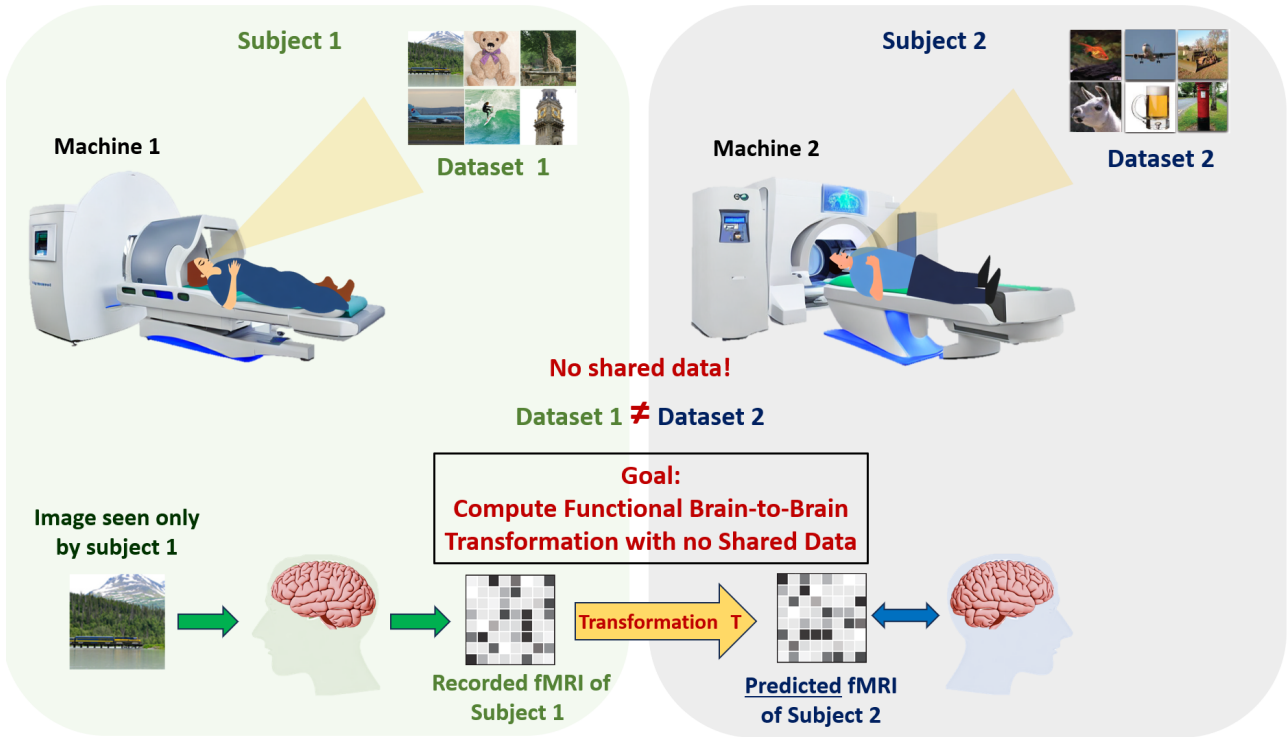


Figure 1: **Problem Formulation - Compute functional brain-to-brain transformation with no shared data:** This figure illustrates our task, learning brain-to-brain transformation between individuals that were exposed to distinct stimuli (images), and their fMRI scans were captured using different fMRI machines (possibly with different scanning resolutions, e.g., 7-Tesla and 3-Tesla).

transformations, thereby exploiting both “non-shared” and “external” data. By leveraging this approach, we significantly enrich the transformation training data. Notably, we demonstrate the capability to compute functional brain-to-brain transformations without any shared images, *even when the fMRI data was collected using different fMRI scanners* (e.g., 7T vs 3T). Furthermore, our results show that we can improve one subject’s image-to-fMRI encoder by utilizing another subject’s encoder, even in the absence of shared data. In particular, we demonstrate the ability to enhance the image-to-fMRI encoding of a subject trained on a low-resolution 3-Tesla fMRI dataset (e.g., “GOD” dataset [23]) by incorporating another subject’s encoder trained on a new 7-Tesla fMRI dataset (e.g., NSD [24]) using our proposed method.

Our contributions are therefore:

- Introducing functional brain-to-brain transformation without the need for shared data, even across distinctly different image datasets and across fMRI scanners of different resolutions (e.g., 7T vs 3T).
- Enhancing the encoding of one subject using data from another high-quality subject (both within and across datasets, e.g., utilizing a subject from a new 7-Tesla dataset to enhance a subject from a low-resolution 3-Tesla dataset).

2 Overview of the Approach

Our approach aims to learn brain-to-brain transformations between subjects (within and across datasets) when subjects were exposed to different stimuli, possibly acquired by different fMRI machines (see Figure 1). We first explain how using visual encoders allows generating “corresponding” fMRI data between different subjects without any shared stimuli. This “corresponding” fMRI data is used to train the transformation. We further demonstrate the effectiveness and applicability of our approach for improving the encoding of one subject using high-quality data from another subject (scanned on a different stimuli dataset and on a different fMRI scanner).

Brain-to-brain transformation with no shared data:

Our approach involves the use of “visual encoders”, which encode images into fMRI signals. These are modeled via deep neural networks, trained on subject-specific image-fMRI pairs. Visuals encoders were shown to obtain impressive accuracy in forecasting a subject’s fMRI responses to novel images [25, 26, 27, 28, 29, 30]. We

first individually train a visual encoder for each subject, utilizing their own respective image-fMRI data (see Figure 2.a). Then, we use the encoder training approach of [30]. Note that such encoder training does **not** require for the two subjects to have experienced the same stimuli; they can belong to entirely distinct image-fMRI datasets.

The functional brain-to-brain transformation T is trained to map the fMRI patterns of Subject1 to their corresponding counterparts in Subject2. The straightforward approach to train the transformation network is to transform an fMRI scan from one subject to match the corresponding fMRI scan of the second subject, and then evaluate its error w.r.t the recorded fMRI (e.g., using the mean square error loss). However, this approach relies on the presence of shared data, and is moot when such shared data is unavailable. Leveraging the predictive capability of the pre-trained encoders for predicting fMRI responses of images, we can generate corresponding fMRI patterns for “non-shared” and “external” images. Given an fMRI scan \mathcal{F}_1 of Subject1, linked to an image \mathcal{I}_1 that only this subject saw (as shown in Figure 2.b on the left side), we can approximate the corresponding fMRI pattern for Subject2 by inputting image \mathcal{I}_1 into the encoder E_2 designed for Subject2. We then optimize the learned transformation T using the fMRI loss between the transformed fMRI $T(\mathcal{F}_1)$ and the encoded fMRI $E_2(\mathcal{I}_1)$, aiming to minimize differences between the two predicted fMRIs ($\|T(\mathcal{F}_1) - E_2(\mathcal{I}_1)\|$). A similar process can be carried out using the fMRI pattern from an image observed solely by Subject2, comparing it against the encoding of the same image using the encoder for Subject1 ($\|T(E_1(\mathcal{I}_\epsilon) - \mathcal{F}_2)\|$). Furthermore, we can incorporate “external” images (depicted in Figure 2.b on the right side). These images are natural images that were never seen by any of the subjects, and thus do not have any fMRI recordings. We feed these “external” images into the encoders of both subjects, subsequently transforming the encoded fMRI pattern of Subject1 and comparing it with the encoded fMRI pattern of Subject2 ($\|T(E_1(\mathcal{I})) - E_2(\mathcal{I})\|$). This provides “infinitely” many training data for *self-supervised training* of the brain-to-brain transformation T .

Improving Image-to-fMRI encoding of one subject using high-quality fMRI of another subject:

To showcase the power of our method, we employ it to enhance the image-to-fMRI encoder of one subject using another subject with superior data quality or more extensive examples. For simplicity, we term this technique the “teacher-student” method, where the subject with higher quality data plays the role of the “teacher”, and the poorer-quality subject is the “student”. This “teacher-student” approach is applicable to subjects of different quality within the same dataset, and more interestingly, it can be employed across different datasets and machines using the above-described method.

We start by training the “teacher” subject’s encoder (E_t) using all its available data. Once trained, we keep its weights unchanged. Then, we simultaneously train the “student” subject’s encoder (E_s) and the transformation T that maps the fMRI data between the “teacher” and “student” subjects ($T_{t \rightarrow s}$). This joint training benefits both the encoder and the transformation, allowing them to improve together. During this step, the “student” encoder is not only trained using its own image-fMRI data, it also incorporates information from the “teacher” encoder and its unique fMRI data (exploit “non-shared” and “external” data). This process is similar to the one shown in Figure 2.b, but with a difference: now, the “student” encoder can be adjusted during training.

For instance, let’s say we take the actual fMRI response from the “teacher” corresponding to an image that the “student” has not encountered before. This response can be transformed to the “student” fMRI space and compared with the encoded response produced by the “student” encoder given that image. Moreover, to make use of “external” data, we can take any image, predict its fMRI using the “teacher” encoder, transform that prediction to the “student” fMRI space, and then compare it with the encoded response of the same “external” image produced by the “student” encoder.

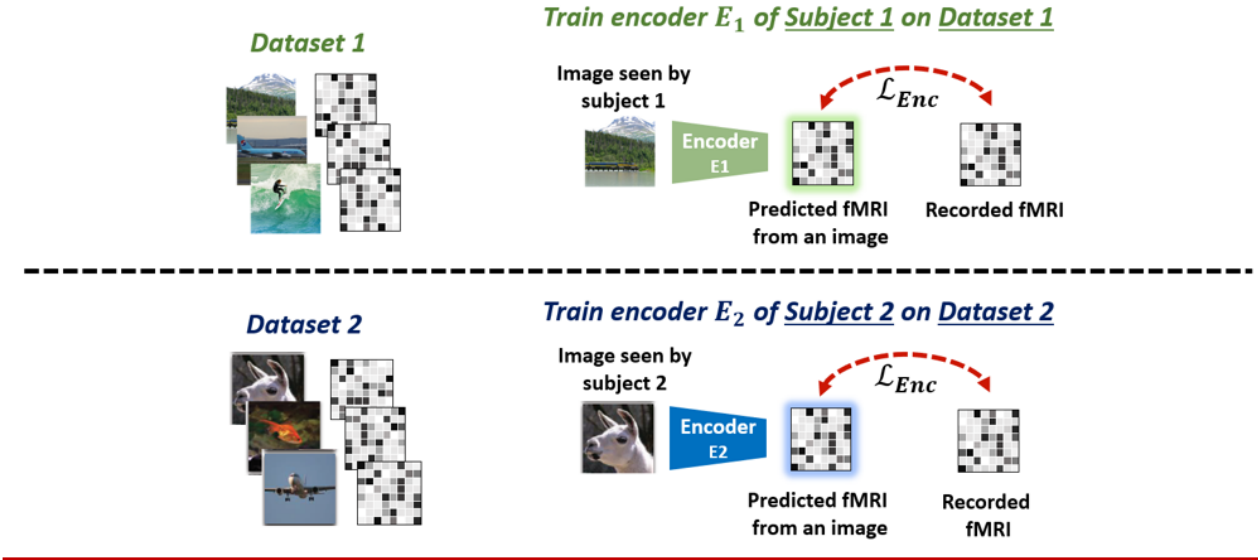
3 Results

We have experimented with three prominent fMRI datasets (see Figure 3): (i) the “vim-1” dataset, which features around 2000 grey-scale images and their corresponding 3-Tesla fMRI recordings for 2 subjects [31, 33, 34]; (ii) the “Generic Object Decoding” (GOD) dataset, which comprises of 1300 pairs of natural images from ImageNet with 3-Tesla fMRI recordings for 5 subjects [32, 35, 36]; and (iii) the “Natural Scenes Dataset” (NSD), a new 7-Tesla dataset with 8 subjects, each having around 1000 shared images and 9000 unique subject-specific images [24] (all in all - 73000 different images).

3.1 Results of Brain-to-Brain Transformation with No Shared Data

This section presents results which substantiate two central claims: (i) Functional transformations can be computed without relying on shared data, yielding significantly better results than anatomical mapping; (ii) Harnessing “non-shared” and “external” images (either alongside or instead of shared data), leads to significantly improved transformations compared to those estimated with shared data.

(a) Training Subject-Specific Image-to-fMRI Encoders (each on its own different dataset)



(b) Learning Functional Transformation with no Shared Data

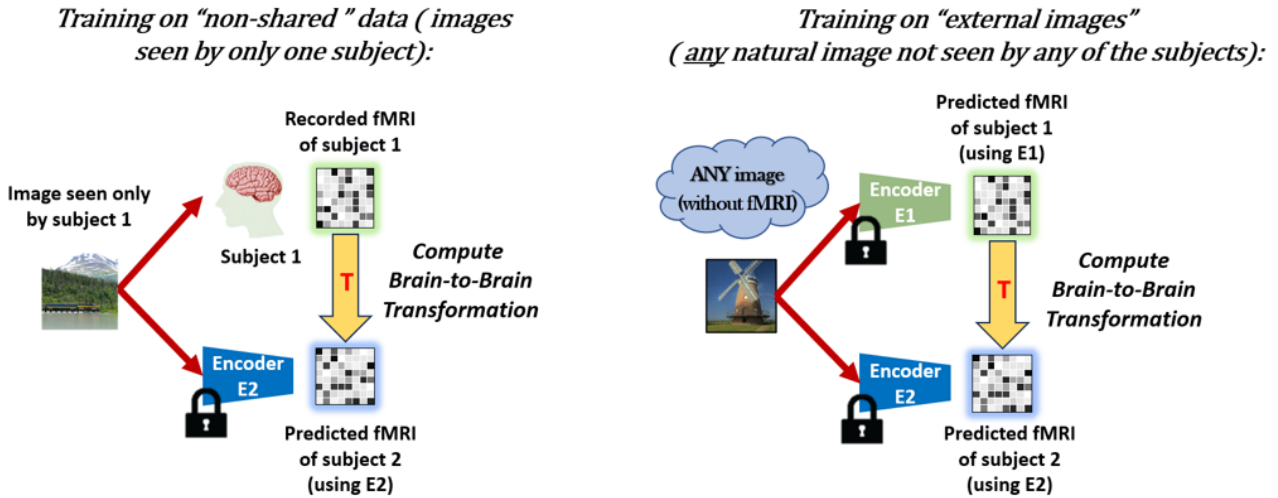


Figure 2: **An overview of the approach - Estimating functional brain-to-brain transformations with no shared data:** (a) Initially, we train separate visual encoders for each subject using its own image-fMRI pairs dataset. Each subject’s data can potentially come from entirely different image datasets and different fMRI scanners. (b) The transformation T is then computed by training a single linear layer to correctly transform fMRI patterns of Subject1 to those of Subject2. We employ the subject-specific pre-trained encoders to predict fMRI responses both for “non-shared” images (i.e, images seen by only one subject), and for “external” images (any natural image never seen by any of the subjects). The large set of predicted fMRIs is then used to train the transformation network T .

FMRI-image datasets used

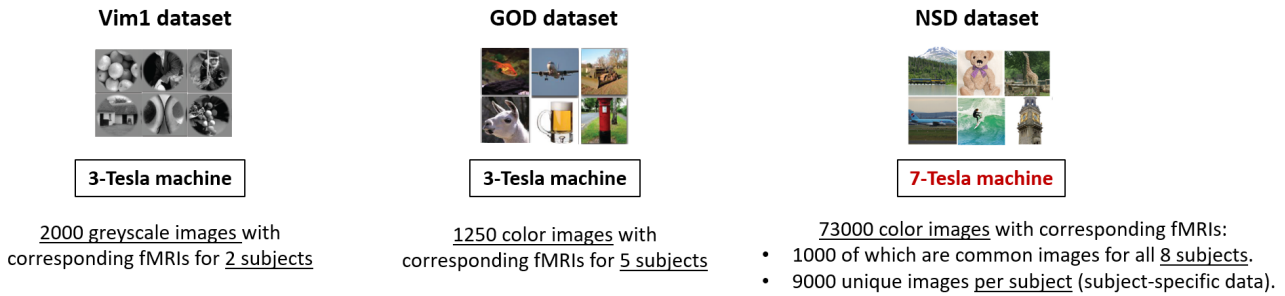


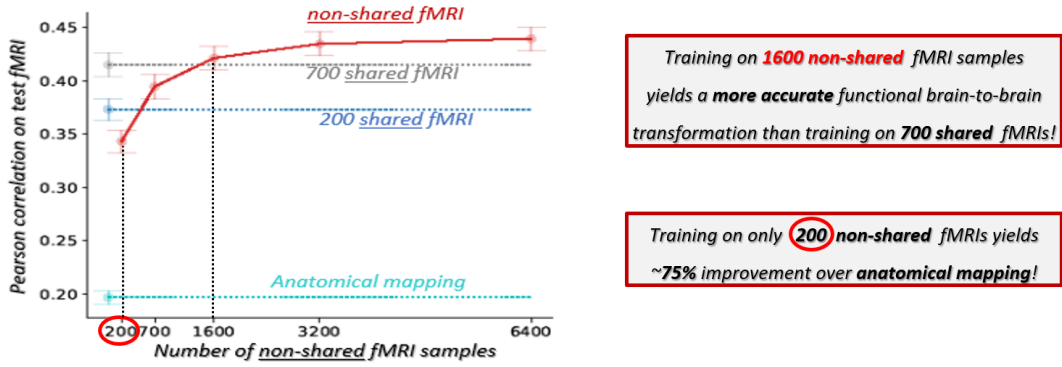
Figure 3: **The fMRI datasets used in our experiments:** (i) “Vim-1” dataset [31] which features grey-scale images and their corresponding 3-Tesla fMRI recordings. (ii) the “Generic Object Decoding” (GOD) dataset [32] which comprises natural ImageNet images with their corresponding 3-Tesla fMRI recordings. (iii) the “Natural Scenes Dataset” (NSD), a new 7-Tesla dataset [24] with 8 subjects, each of whom viewed 1000 shared images and 9000 unique subject-specific images.

To validate these claims, we use the NSD dataset. This dataset offers a relatively limited number of shared data (1000 shared images) and a substantial number of non-shared data (9000 images per subject), rendering it well-suited for illustrating our claims. Given that we possess both non-shared and shared data, we can exclusively train a transformation model using non-shared data and then assess its performance on a dedicated evaluation set of shared data. We evaluate the quality of the learned transformation T in 2 ways: (i) Quantitatively, we measure the Pearson correlation between the predicted fMRI (i.e., the fMRI obtained by transforming the source subject’s fMRI to the target subject’s space) and the actual fMRI of the target subject; (ii) Qualitatively, we assess the content of the transformed fMRI through an fMRI decoder (mapping fMRI to images), and visually inspect the quality of the decoded images. This decoding is achieved by combining 2 fMRI-to-image decoding methods [30] and [37] (for further details, please refer to the Supplementary Material).

Quantitative evaluation: The graph in Figure 4.a presents the mean Pearson’s r correlation averaged over all 56 transformations of all possible pairs of subjects in the NSD dataset. We compare the resulting transformations when trained only with non-shared data (solid red line) to three other transformations: an anatomical mapping to a common brain space (cyan dotted line), a transformation trained with only 200 shared examples (dotted blue line), and a transformation trained with 700 shared examples (dotted grey line). The remaining 300 “shared data” serve as “test data” for assessing and comparing the quality of all the learned transformations. The x-axis of the graph represents the number of non-shared examples available for training, where our transformation model is the only one that can use non-shared examples. When there are no shared examples, we can only compare our method to anatomical alignment. As seen from the graph, our approach performs significantly better than anatomical alignment, even with small amounts of non-shared examples ($df = 56$, $t = 18.57$, $p < 1e - 20$, $d = 2.48$; up to 75% improvement when training with as little as 200 non-shared examples). Furthermore, our method, when utilizing only non-shared examples, yields comparable or even better results than transformation models trained with shared data. As we increase the number of non-shared examples, the transformation model’s performance continues to improve, surpassing models trained with only 200 and 700 shared examples. Although shared data is more beneficial when there is a low number of examples, 700 non-shared examples ($M=0.407$, $SD=0.07$) perform better than 200 shared examples ($M=0.385$, $SD=0.07$, $df = 56$, $t = 12.08$, $p < 5e - 17$, $d = 1.61$), and 1600 non-shared examples ($M=0.4349$, $SD=0.07$) perform better than all 700 shared examples ($M=0.429$, $SD=0.07$, $df = 56$, $t = 3.32$, $p = 2e - 3$, $d = 0.44$). This is because, with sufficient examples, the encoder used for our training of the transformation is robust enough to compensate for the absence of shared examples. We provide specific transformations with mean Pearson’s r correlation values in Figure ?? in the Supplementary Material. Figures ?? and ?? further demonstrate that combining non-shared examples with available shared examples leads to better results than using shared examples alone.

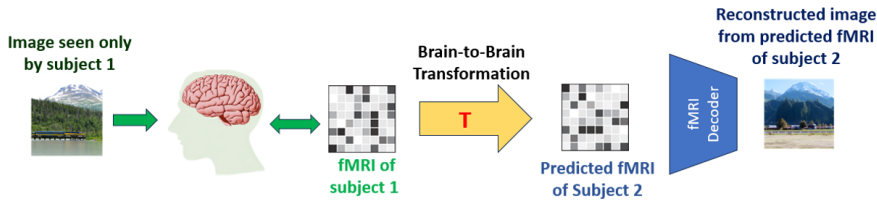
Qualitative evaluation: Figure 4.b further provides a visual comparison of visual decoding when using our transformation model versus anatomical alignment method (the only two possible methods for handling non-shared data). The transformation is used to map the fMRI activity of Subject1 to predict the fMRI activity of Subject2. We then utilize a pre-trained decoder [30] of Subject2 (trained on its unique data), together with a novel diffusion model decoding approach [37] to generate images from the transformed fMRI. The figure displays the original image seen by Subject1, along with two reconstructed images post fMRI transformation from Subject1 to Subject2: Once using anatomical mapping between the subjects, and once using our transformation

(a) *Quantitative evaluation: Voxel Pearson correlation between transformed fMRI and recorded fMRI*



(b) *Qualitative evaluation: Image reconstruction from the of transformed fMRI*

Overview of evaluation process:



Examples of reconstructed images from transformed fMRI:

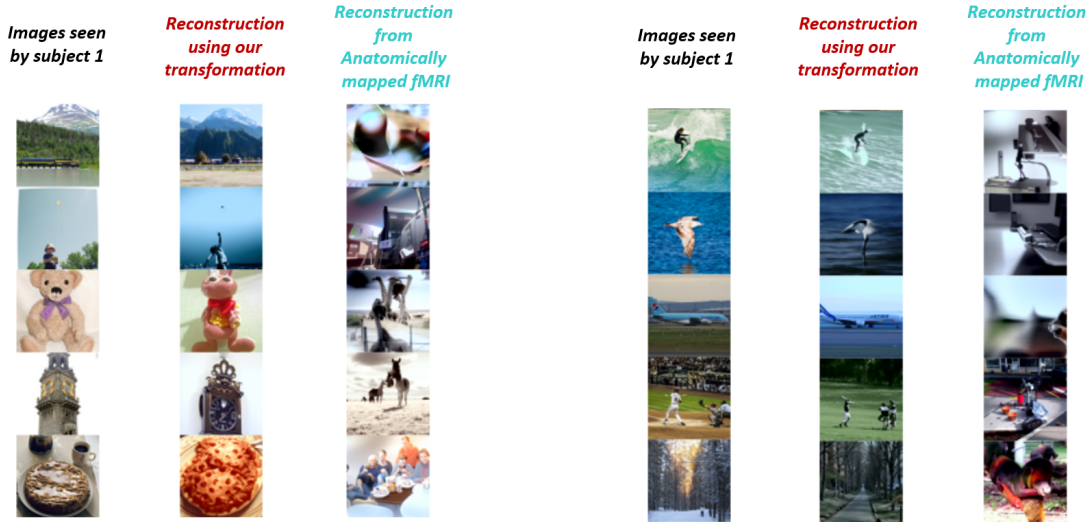


Figure 4: **Evaluating brain-to-brain transformation with no shared data:** (a) Quantitative evaluation: The graph presents the mean Pearson’s r correlation averaged over all 56 transformations of all possible pairs of subjects in the NSD dataset, with SEM (standard error of the mean) error bars. We compare the resulting transformations when trained only with non-shared data (solid red line) to three other transformations: an anatomical mapping to a common brain space (cyan dotted line), a transformation trained with only 200 shared examples (dotted blue line), and a transformation trained with 700 shared examples (dotted grey line). The remaining 300 “shared data” serve as “test data” for assessing and comparing the quality of all the learned transformations. The x-axis of the graph represents the number of non-shared examples available for training, where our transformation model is the only one that can use non-shared examples. (b) Qualitative evaluation: This figure provides a visual comparison of image decoding when using our transformation model versus anatomical alignment method (the only 2 possible methods for handling non-shared data). As can be seen in the diagram, the transformation is used to map the fMRI activity of Subject1 to predict the fMRI activity of Subject2. Then we utilize the pre-trained decoder [30] of Subject2 (trained on his mutually exclusive data), together with a novel diffusion model decoding approach [37] to generate images from the transformed fMRI. The figure displays the original image seen by Subject1, along with two reconstructed images post-fMRI transformation from Subject1 to Subject2: Once using anatomical mapping between the subjects, and once using our transformation model T trained without any shared data.

model T trained without any shared data. This demonstrates that our transformation produces fMRI predictions with more relevant and semantically meaningful information for reconstructing images. This visual comparison underscores that our transformation, trained without shared data, generates significantly superior outcomes compared to anatomical mapping, the only technique used to-date when shared data is absent. For additional reconstructions and transformations, please refer to Figures ?? and ?? in the Supplementary Material.

3.2 Improving Image-to-fMRI Encoding of one Subject using another Higher-Quality Subject

We next demonstrate how our transformation method allows one subject from a high quality fMRI dataset (the “teacher”) to improve the image-to-fMRI encoding capabilities of another subject from a low quality fMRI dataset (the “student”). Normally there are no shared images across different fMRI datasets, in which case our transformation method is needed. This applies also when both subjects are from the same dataset, but one subject has higher fMRI quality than the other.

Figure 5 compares the quality of the “student” baseline encoder (which is trained solely on the student’s own fMRI data), to the student encoder obtained when incorporating also data from the “teacher” during training. The student encoder benefits from the unique fMRI data of the teacher (the subject with higher-quality data, e.g., from NSD 7 Tesla dataset), as well as from images that neither subjects have encountered (via the “teacher” higher quality encoder). This data is used in addition to the student’s own fMRI data. Improvements of subjects’ encoders from the GOD 3-Tesla dataset are depicted in Figure 5. In each plot, the grey line represents the student baseline encoder model, the purple line symbolizes the encoder improvement obtained when using a “teacher” from the same dataset (e.g., Subject4 is the highest-quality subject in the GOD dataset). The orange line corresponds to the encoder improvement achieved by utilizing a superior subject from another dataset (NSD), which has more scanned examples and higher fMRI resolution (7-Tesla machine).

The quality of the resulting encoders is assessed through the mean Pearson correlation of all predicted fMRI voxels. The “number of training examples” refers to the number of the student’s own image-fMRI pairs of examples used for training the “student” encoder (Subject1 from GOD dataset), whereas the “teacher” encoder (of a different subject from either GOD or NSD dataset) has been trained using all its own available examples and remains unchanged during the training of the student encoder.

Figure 5.a shows the results for an individual subject (Subject1), and Figure 5.b aggregates the results of all five subjects in GOD dataset (showing mean values and SEM). Both graphs show that encoders trained with a “teacher” subject exhibit significant improvement over their baseline encoder. Notably, employing Subject4 from the same dataset as a “teacher” results in a substantial improvement of approximately 50% ($df = 20$, $t = 8.15$, $p < 5e - 7$, $d = 1.82$). Remarkably, utilizing a subject from the higher-resolution NSD dataset as a “teacher” leads to even more pronounced performance gains. Specifically, for a small number of examples, it demonstrates a nearly 100% relative improvement over the baseline encoder, and 50% over the other enhanced encoder model ($df = 20$, $t = 5.85$, $p < 5e - 5$, $d = 1.31$). These observations are remarkable given that the NSD dataset does not share images with the GOD dataset, whereas a “teacher” subject from the same dataset shares numerous images with the “student” subject. Supplementary examples showcasing the improvement of specific subjects’ encoders are provided in Figure ?? in the Supplementary Material.

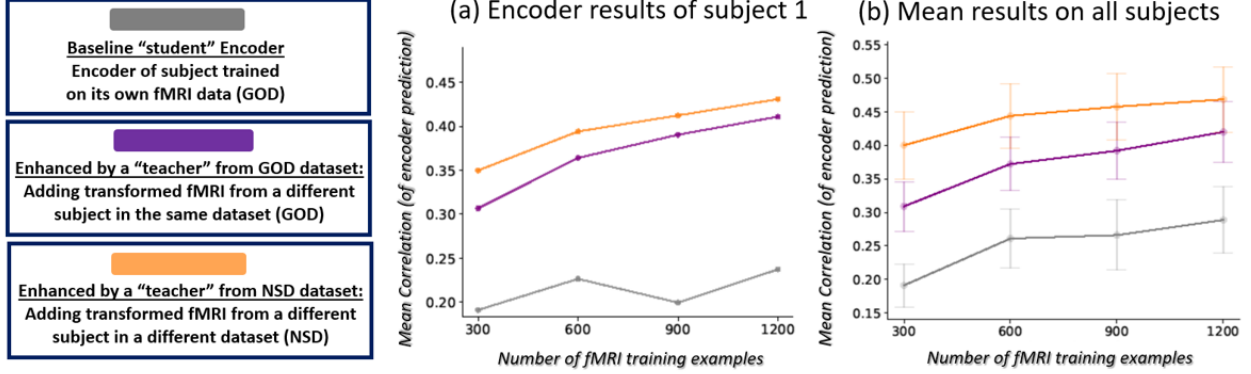
Lastly, Figure 5.c presents the distribution of Pearson correlations across the fMRI voxels, comparing the baseline student encoder against the improved student encoder when trained with a teacher from the NSD dataset. This is evaluated using varying numbers of training examples (300, 600, and 1200) from the student’s own fMRI data. As the figure indicates, our enhanced encoder (depicted by the orange histogram) shifts the distribution to the right, signifying the improved correlation in a substantial portion of fMRI voxels.

Next, we present our results on the old Vim-1 fMRI dataset, which contains only two subjects who observed grey-scale images. Given the limited subject number, we showcase the method using a “teacher” subject drawn from other datasets, namely GOD and NSD. Figure 6.a and 6.b shows the results for each individual subject. As in Figure 5, the grey line represents the student baseline encoder, the purple line symbolizes the encoder improvement obtained using as a “teacher” from the GOD dataset. The orange line corresponds to the encoder improvement achieved by utilizing a superior subject from the higher fMRI resolution dataset (NSD). Both plots show that encoders trained with a “teacher” subject exhibit an improvement over their baseline encoder model. The results illustrate that, as expected, a subject from the NSD 7-Tesla dataset, when used as a “teacher”, outperforms using a “teacher” subject from the GOD 3-Tesla dataset. Notably, despite the considerable differences between the “teacher” and “student” subjects in terms of data characteristics (color vs grey-scale images, different image datasets), the method remains effective in leveraging one subject’s higher-quality data to improve another.

Lastly, Figure 6.c presents the distribution of Pearson correlations across the fMRI voxels, comparing the baseline student encoder against the improved student encoder when trained with a teacher from the NSD dataset. This is evaluated using varying numbers of training examples (300, 900, and 1750) from the student’s

Evaluation of Encoder Improvement – GOD Dataset

Encoders of GOD 3-Tesla Dataset Improved by NSD 7-Tesla Dataset



(c) Pearson Correlation Distribution of fMRI Voxels Predicted via Student Encoder: Student Baseline Encoder vs Student Enhanced Encoder(via a teacher from NSD)

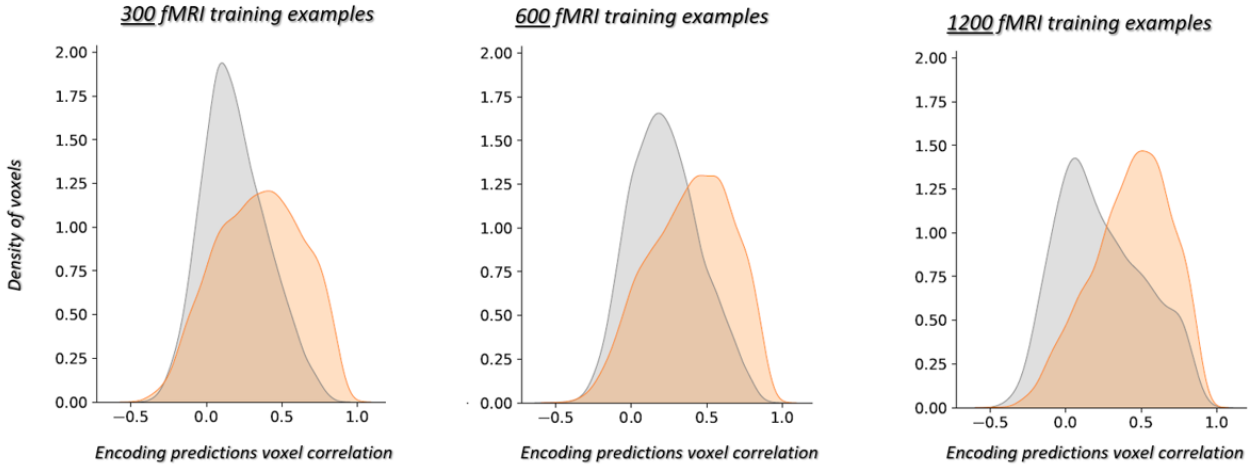
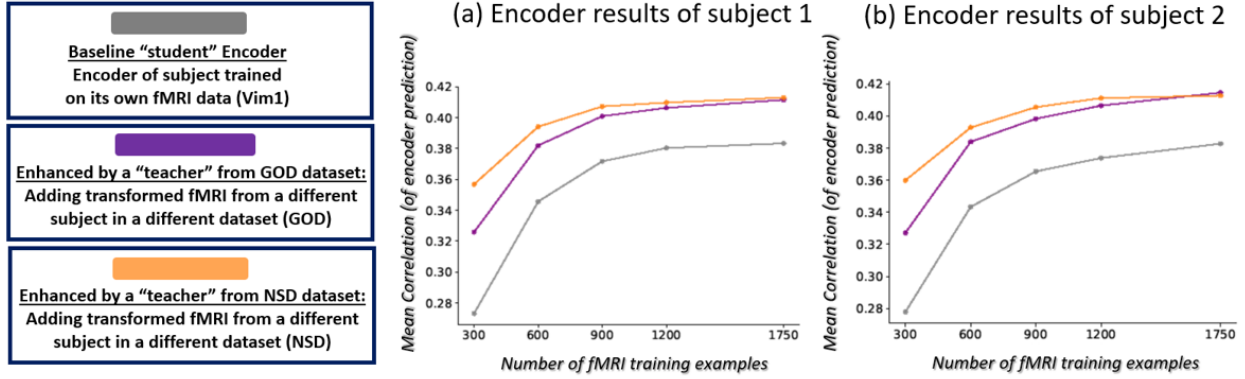


Figure 5: **Improving encoding of a subject from GOD 3-Tesla dataset (“student”) using another high-quality subject (“teacher”)**: This figure compares the quality of the “student” baseline encoder (which is trained solely on the student’s own fMRI data) to the student encoder obtained when incorporating also data from the “teacher” during training. In each plot, the grey line represents the student baseline encoder model, the purple line symbolizes the encoder improvement obtained when using a “teacher” from the same dataset (e.g., Subject4 is the highest-quality subject in the GOD dataset). The orange line corresponds to the encoder improvement achieved by utilizing a superior subject from another dataset (NSD), which has more scanned examples and higher fMRI resolution (7-Tesla machine). The quality of the resulting encoders is assessed through the mean Pearson correlation of all predicted fMRI voxels. The “number of training examples” refers to the number of the student’s own image-fMRI pairs of examples used for training the “student” encoder, whereas the “teacher” subject (drawn from either GOD or NSD dataset) has been trained using all its own available examples and remains unchanged during the training of the student encoder. **(a)** Results for an individual student subject (Subject1). **(b)** Aggregated results of all five subjects in GOD dataset (displaying mean values and SEM error bars). **(c)** The distribution of Pearson correlations across the fMRI voxels, comparing the baseline student encoder against the improved student encoder when trained with a teacher from the NSD dataset. This is evaluated using varying numbers of training examples (300, 600, and 1200) from the student’s own fMRI data. The x-axis signifies the Pearson correlation values, while the y-axis represents the density of fMRI voxels corresponding to each correlation value.

Evaluation of Encoder Improvement – Vim1 Dataset

Encoders of Vim1 3-Tesla Dataset Improved by other Datasets



(c) Pearson Correlation Distribution of fMRI Voxels Predicted via Student Encoder: Student Baseline Encoder vs Student Enhanced Encoder(via a teacher from NSD)

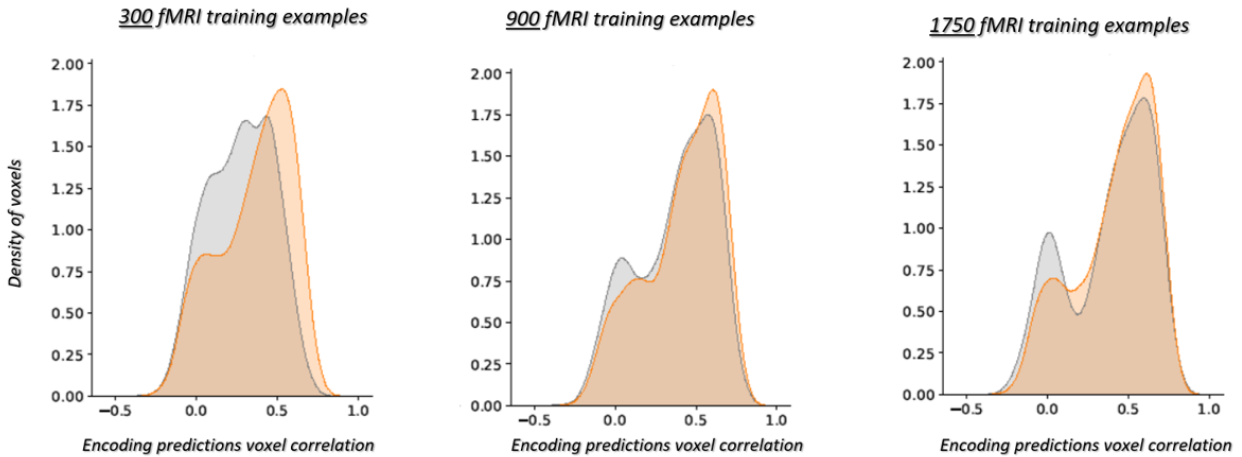


Figure 6: **Improving encoding of a subject from Vim1 3-Tesla dataset (“student”) using another high-quality subject (“teacher”):** This figure compares the quality of the “student” baseline encoder (which is trained solely on the student’s own fMRI data), to the student encoder obtained when incorporating also data from the “teacher” during training. In each plot, the grey line represents the student baseline encoder model, the purple line symbolizes the encoder improvement derived using as a “teacher” from the GOD dataset (e.g., Subject4 is the highest-quality subject in the GOD dataset). The orange line corresponds to the encoder improvement achieved by utilizing a superior subject from another dataset (NSD), which has more scanned examples and higher fMRI resolution (7-Tesla machine). The quality of the resulting encoders is assessed through the mean Pearson correlation of all predicted fMRI voxels. The “number of training examples” refers to the number of the student’s own image-fMRI pairs of examples used for training the “student” encoder, whereas the “teacher” subject (drawn from either GOD or NSD dataset) has been trained using all its own available examples and remains unchanged during the training of the student encoder. (a) Results for an individual student subject (Subject1). (b) Results for an individual student subject (Subject2). (c) The distribution of Pearson correlations across the fMRI voxels, comparing the baseline student encoder against the improved student encoder when trained with a teacher from the NSD dataset. This is evaluated using varying numbers of training examples (300, 900, and 1750) from the student’s own fMRI data. The x-axis signifies the Pearson correlation values, while the y-axis represents the density of fMRI voxels corresponding to each correlation value.

Zero-Shot Classification of Novel Semantic Classes : Classification by GOD subjects using Improved Encoder

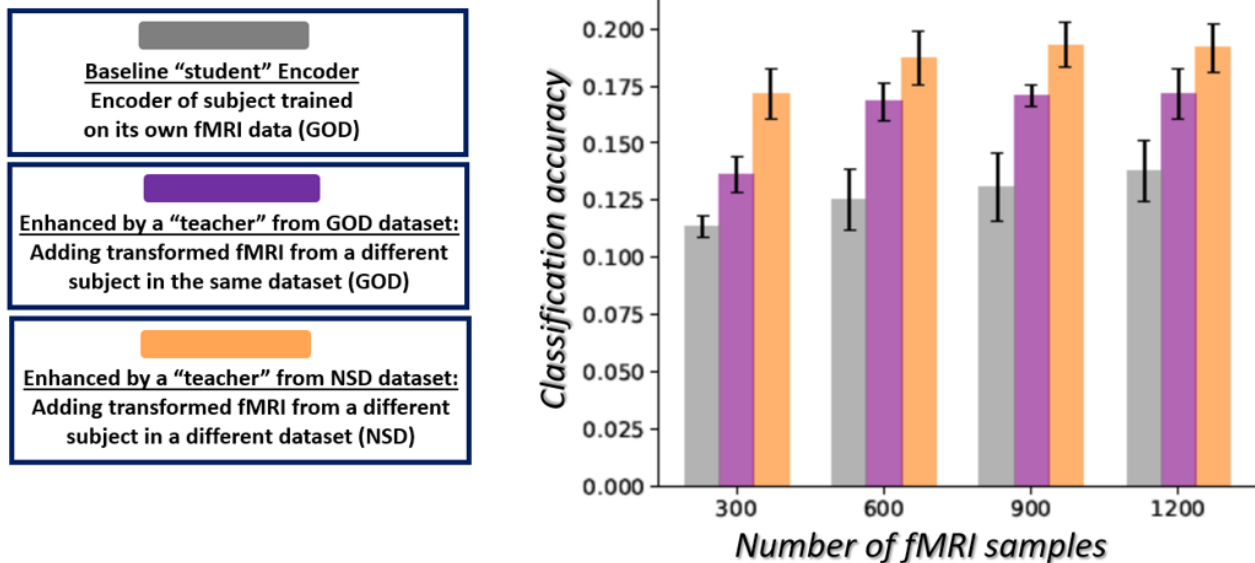


Figure 7: **Improving classification accuracy (of never-before-seen image classes) of a 3-T GOD subject, using its enhanced encoder via another subject:** This plot presents the classification results employing this approach, considering different modes of encoder training. We compare the baseline encoder (trained only on its subject-specific fMRI data) with encoders improved by another subject (“teacher”), either from the GOD dataset or using the NSD 7-Tesla dataset. The results presented are the mean accuracy of all subjects with the SEM error.

own fMRI data. As the figure indicates, our enhanced encoder (depicted by the orange histogram) shifts the distribution to the right, signifying the improved correlation in a substantial portion of fMRI voxels.

We further examined the usefulness of our improved encoders (compared to baseline encoders) for “Zero-Shot” classification (i.e., classification of fMRI data to novel image categories, which were never-before-seen during training). The classification method we used is similar to that of [30] (with some small modifications), and is described in the supplementary text and in Figure ?? . Figure 7 compare the classification performance using different encoders. The results indicate that, irrespective of the number of training examples, the enhanced encoders (represented by the purple column) achieve significantly higher classification accuracy than the baseline encoders (grey column), as confirmed by statistical analysis (paired samples student’s t-test, $df = 20$, $t = 4.69$, $p < 5e - 5$, $d = 1.05$). Furthermore, the application of an enhanced encoder trained with the 7-Tesla dataset (orange column) demonstrates even greater classification accuracy, supported by a t-test comparison with the GOD 3-Tesla “teacher” ($df = 20$, $t = 3.76$, $p < 5e - 3$, $d = 0.84$). Additionally, Figure ?? includes results showing the improved brain-to-brain transformations within the GOD dataset capability of the improved encoder to incorporate “external” images with shared data, further underscoring their effectiveness in enhancing various tasks in lower-resolution datasets.

4 Discussion

This paper introduces, for the first time, an approach to learn functional brain-to-brain transformations between different subjects without requiring any shared data. Our methods hold the potential to significantly enhance research in brain functionality, expanding both the quantity and quality of data available for analysis. This breakthrough offers exciting research opportunities, enabling the merging and enrichment of diverse datasets, even when they involve different stimuli or were collected using fMRI machines of varying resolutions.

Beyond the novel method for computing brain transformations without shared data, our innovation also lies in the integration of visual encoders with these transformations. We can now utilize both “non-shared” and “external” images for training encoders and transformations. This ability to incorporate images unseen by any of the subjects marks a significant advancement, greatly expanding the capacity of training data for various different fMRI related tasks.

Our method is particularly effective in utilizing new high-quality fMRI datasets, such as the NSD 7-Tesla

dataset, to enhance older, lower-quality datasets like the GOD and Vim1 3-Tesla datasets. We have demonstrated substantial improvements in image-to-fMRI encoding with low-resolution 3T datasets. These enhanced encoders further enable improvements in within-dataset brain-to-brain transformations and boost the accuracy of semantic classification for novel, never-before-seen image categories. These enhancements are particularly exciting, offering the potential to significantly advance our understanding of how the brain perceives and processes visual information. Altogether, this underscores the importance of our method in improving older datasets by leveraging newer, high-quality datasets.

Importantly, our approach is general, hence can be extended to other modalities (e.g., MEG, EEG, ECoG), as well as to other stimulus types (e.g., audio, video, text). We further believe that our proposed approach has numerous potential applications, which may advance our understanding of the brain and its functions.

5 Methods

5.1 Datasets

We tested our approach on three distinct publicly available fMRI datasets: “Natural Scenes Data set“ (NSD) [24], Generic Object Decoding (GOD) [23], and “Visual Imaging 1” (Vim1) [31, 33]. The datasets provide fMRI responses of human subjects to a variety of natural images. In all the experiments, the participants were instructed to fixate their eyes on the center of the presented images. We summarize differences between the datasets in Table 1.

Natural Scenes Dataset (NSD) is a new dataset recorded using 7-Tesla fMRI machine, resulting in higher voxel resolution. All 8 subjects in this dataset were presented with 1,000 shared images and 9,000 unique images per subject. This is contrary to other datasets where all participants were presented the same stimuli. Vim1 dataset has grey scale stimuli images with a circular mask (see Figure 3), whereas the other datasets that have RGB images. It should be noted that each dataset was scanned with a different machine as well as different recording scheme and processing protocols. We use the same approach and architecture to produce results for all the datasets. In addition to the fMRI datasets, we also used 50,000 natural images as “External Images” (images without any fMRI). Those images were taken from 1000 classes of ImageNet validation data (“ILSVRC” [38]). Those images are the “external” data reported in our experiments.

Dataset	Number of distinct stimuli	Number of subjects	Machine resolution	Image origin
NSD [24]	10000 per subject (73000 total)	8	7T	COCO [39]
GOD [23]	1250 per subject (1250 total)	5	3T	ImageNet [38]
Vim1 [31, 33]	2000 per subject (2000 total)	2	3T	Multiple sources

Table 1: Summary of fMRI datasets used in the paper.

5.2 Technical Details of the Method

5.2.1 Training brain-to-brain transformations with no shared data

The brain-to-brain transformation at the core of our method is implemented via a simple neural architecture featuring a single linear layer, optimized with an L2 regularization loss (detailed below). The image-to-fMRI encoder employed in our work is based on the framework outlined in [30]. It encompasses a pre-trained VGG network augmented with additional convolution layers and a non-linear layer to project data into the fMRI space. Prior to training the transformation network T , we performed separate training for the visual encoder of each subject individually (on their individual data), using the procedure recommended in [30] (refer to Figure 2.a). Notably, during transformation training, the encoder weights remained fixed.

The transformation T serves the purpose of mapping fMRI patterns from one subject (Subject1) to their corresponding patterns in another subject (Subject2). Leveraging the predictive capability of the pre-trained encoders for forecasting fMRI responses to images, we are capable of generating corresponding fMRI patterns for “non-shared” and “external” images. These are used to train the transformation T , without any shared data between the two subjects.

Our fMRI loss function adopts the mean square error loss between fMRIs:

$$\mathcal{L}_{fMRI}(\hat{x}, x) = \|\hat{x} - x\|_2$$

where x is the target fMRI, and \hat{x} is the predicted fMRI after applying the transformation T .

Our overall training loss encompasses three components corresponding to different data types (shared, non-shared, and external), and in each scenario, we can use all or only some of them together. Each component

employs the same fMRI loss metric, with variations in the types of fMRI data compared (shared, non-shared, or external) and the coefficients assigned. A regularization term \mathcal{L}_{Reg} employs L2 regularization on the weights of the linear transformation layer, aligning with prior methods [15]. The total loss, can be represented as follows:

$$\mathcal{L} = \alpha_S \mathcal{L}_S + \alpha_{NS} \mathcal{L}_{NS} + \alpha_{Ext} \mathcal{L}_{Ext} + \alpha_{Reg} \mathcal{L}_{Reg}$$

The first loss term, \mathcal{L}_S , leverages “shared data”:

$$\mathcal{L}_S = \mathcal{L}_{fMRI}(T_{1,2}(F_1), F_2)$$

where F_1 represents the recorded fMRI of Subject1, and F_2 represents the recorded fMRI of Subject2, while observing the same image. $T_{1,2}$ denotes the transformation model mapping from Subject1 to Subject2. We employ the fMRI loss of the transformation to compare the transformed fMRI with the actual measured fMRI.

The second loss term, \mathcal{L}_{NS} , utilizes “non-shared data” (refer to Figure 2.b):

$$\mathcal{L}_{NS} = \mathcal{L}_{fMRI}(T_{1,2}(F_1), E_2(I_1)) \text{ or } \mathcal{L}_{NS} = \mathcal{L}_{fMRI}(T_{1,2}(E_1(I_2)), F_2)$$

where F_1 and I_1 correspond to the recorded fMRI of Subject1 and the corresponding image (the image viewed exclusively by Subject1). We transform Subject1’s fMRI signals and compare them to the encoded fMRI signals derived from the image seen by Subject1(using Subject2’s encoder). In the same manners, F_2 and I_2 correspond to the recorded fMRI of Subject2 and the corresponding image (the image viewed exclusively by Subject2). We transform the encoded fMRI signals derived from the image seen by Subject2(using Subject1’s encoder) and compare them to Subject2’s fMRI signals F_2 .

The third loss term, \mathcal{L}_{Ext} , involves “External” images (refer to Figure 2.c):

$$\mathcal{L}_{Ext} = \mathcal{L}_{fMRI}(T_{1,2}(E_1(I_{Ext})), E_2(I_{Ext}))$$

In this case, I_{Ext} represents an external image with no corresponding fMRI data for any of the subjects. We feed this image into the encoders of both subjects. After encoding the fMRI, the loss is similar to that in the case of \mathcal{L}_S , utilizing the encoded fMRI.

It is worth noting that the number of shared and non-shared fMRI data is constrained by the available data, while the number of external images is essentially limitless. In occasions where we train the transformation without any shared data, either within or between datasets, we omit the first loss term \mathcal{L}_S and employ only the other two loss components (\mathcal{L}_{NS} and \mathcal{L}_{Ext}).

The coefficients governing the three loss terms and the regularization factor are established through a validation process. We separate the fMRI data into 3 sets: Train (80%), Validation(10%) and Test (10%). Subsequently, we select the optimal coefficients by assessing the transformation model performance on the validation set.

5.2.2 Improving Image-to-fMRI encoding of one subject using another subject’s fMRI

We enhance the image-to-fMRI encoder of one subject using another subject with superior data quality or more extensive examples. For simplicity, we term this technique the “teacher-student” method, where the subject with higher quality data plays the role of the “teacher”, and the poorer-quality subject is the “student”.

The process initiates by training the “teacher” subject’s encoder (E_t) using its complete dataset, with the resulting weights remaining unchanged. Following this, we engage in simultaneous training of the “student” subject’s encoder (E_s) and the transformation responsible for mapping fMRI data between the “teacher” and “student” subjects ($T_{t,s}$). This joint training benefits both the encoder and the transformation, allowing them to improve collaboratively. Importantly, during this step, the “student” encoder is not solely trained on its own data but also incorporates information from the “teacher” encoder and its unique (often non-shared) fMRI data, as well as “external” data (images without any fMRI).

Our comprehensive loss function comprises three components corresponding to different data types (shared, non-shared, and external). In each scenario, we can choose to use all or only some of these components together. Additionally, we include an encoding loss, which pertains to the student encoder and its available data. Lastly, a regularization term \mathcal{L}_{Reg} employs L2 regularization on the weights of the linear transformation layer. Our loss function can be represented as follows:

$$\mathcal{L} = \alpha_{Enc} \mathcal{L}_{Enc} + \alpha_S \mathcal{L}_S + \alpha_{NS} \mathcal{L}_{NS} + \alpha_{Ext} \mathcal{L}_{Ext} + \alpha_{Reg} \mathcal{L}_{Reg}$$

The first loss, \mathcal{L}_{Enc} , calculates the student encoding loss using all the available image-fMRI pairs of the student subject:

$$\mathcal{L}_{Enc} = \mathcal{L}_{fMRI}(E_{Student}(I_{Student}), F_{Student})$$

In this equation, $I_{Student}$ and $F_{Student}$ represent the image-fMRI pairs of the student subject. The loss measures the discrepancy between the encoded image (by the student encoder) and the actual measured fMRI using the fMRI encoding loss.

The second loss, \mathcal{L}_S , is similar to the shared data loss from the previous section. It calculates the transformation loss based on all the shared fMRI-fMRI pairs in the dataset, corresponding to both the student and the teacher.

Subsequently, we have two additional losses, \mathcal{L}_{NS} and \mathcal{L}_{Ext} (see Figure 2.b and 2.c), calculated in a manner similar to that presented in the previous section, with the distinction that the student encoder weights are not fixed and are affected by the training process. For instance, if we consider the scenario of \mathcal{L}_{NS} , we take the actual fMRI response $F_{Teacher}$ from the “teacher” corresponding to an image $I_{Teacher}$ that the “student” has never seen before. This response is then transformed to the “student’s” fMRI space and compared to the encoded response produced by the “student” encoder for the same image. Namely:

$$\mathcal{L}_{NS} = \mathcal{L}_{fMRI}(E_{Student}(I_{Teacher}), F_{Teacher})$$

Similarly for any external image I :

$$\mathcal{L}_{Ext} = \mathcal{L}_{fMRI}(E_{Student}(I), E_{Teacher}(I))$$

The choice of the “teacher” subject is a crucial step in our method. We select the “teacher” subject based on its encoder’s performance when individually trained on its own data and evaluated on a validation set. The subject with the best-performing encoder is chosen for this role. Notably, the “teacher” subject can be selected from the same dataset or even from a different dataset, depending on the specific application.

To determine the optimal coefficients for the loss functions and regularization, we employ a validation procedure, as outlined in a previous section.

When applying our method to the “Vim1” dataset and the NSD dataset, we encountered a few challenges. These datasets differ in terms of color representation, with one being grey-scale and the other in RGB format. To bridge this domain gap, we converted the external and non-shared images to grey-scale, minimizing disparities between them.

6 Data availability

All the datasets analysed during the current study are publicly available. The NSD dataset is available through <https://naturalscenesdataset.org> with access agreement submission. The GOD dataset is available in the “GenericObjectDecoding” repository, <https://github.com/KamitaniLab/GenericObjectDecoding>. The Vim1 dataset is available in <https://crcns.org/data-sets/vc/vim-1/about-vim-1>.

References

- [1] Nancy Kanwisher, Josh McDermott, and Marvin M Chun. The fusiform face area: a module in human extrastriate cortex specialized for face perception. *Journal of neuroscience*, 17(11):4302–4311, 1997.
- [2] Russell Epstein and Nancy Kanwisher. A cortical representation of the local visual environment. *Nature*, 392(6676):598–601, 1998.
- [3] Paul E Downing, Yuhong Jiang, Miles Shuman, and Nancy Kanwisher. A cortical area selective for visual processing of the human body. *Science*, 293(5539):2470–2473, 2001.
- [4] I-Chun Tang, Yu-Ping Tsai, Ying-Ju Lin, Jyh-Horng Chen, Chao-Hsien Hsieh, Shih-Han Hung, William C Sullivan, Hsing-Fen Tang, and Chun-Yen Chang. Using functional magnetic resonance imaging (fmri) to analyze brain region activity when viewing landscapes. *Landscape and Urban Planning*, 162:137–144, 2017.
- [5] David J Heeger and David Ress. What does fmri tell us about neuronal activity? *Nature reviews neuroscience*, 3(2):142–151, 2002.
- [6] DR Riddle and Dale Purves. Individual variation and lateral asymmetry of the rat primary somatosensory cortex. *Journal of Neuroscience*, 15(6):4184–4195, 1995.
- [7] Martin A Frost and Rainer Goebel. Measuring structural–functional correspondence: spatial variability of specialised brain regions after macro-anatomical alignment. *Neuroimage*, 59(2):1369–1381, 2012.
- [8] Bryan R Conroy, Benjamin D Singer, J Swaroop Guntupalli, Peter J Ramadge, and James V Haxby. Inter-subject alignment of human cortical anatomy using functional connectivity. *NeuroImage*, 81:400–411, 2013.

- [9] Zonglei Zhen, Zetian Yang, Lijie Huang, Xiang-zhen Kong, Xu Wang, Xiaobin Dang, Yangyue Huang, Yiying Song, and Jia Liu. Quantifying interindividual variability and asymmetry of face-selective regions: a probabilistic functional atlas. *Neuroimage*, 113:13–25, 2015.
- [10] John Mazziotta, Arthur Toga, Alan Evans, Peter Fox, Jack Lancaster, Karl Zilles, Roger Woods, Tomas Paus, Gregory Simpson, Bruce Pike, et al. A probabilistic atlas and reference system for the human brain: International consortium for brain mapping (icbm). *Philosophical Transactions of the Royal Society of London. Series B: Biological Sciences*, 356(1412):1293–1322, 2001.
- [11] J Talairach. 3-dimensional proportional system; an approach to cerebral imaging. co-planar stereotaxic atlas of the human brain. *Thieme*, pages 1–122, 1988.
- [12] Bruce Fischl. Freesurfer. *Neuroimage*, 62(2):774–781, 2012.
- [13] Anders M Dale, Bruce Fischl, and Martin I Sereno. Cortical surface-based analysis: I. segmentation and surface reconstruction. *Neuroimage*, 9(2):179–194, 1999.
- [14] James V Haxby, J Swaroop Guntupalli, Andrew C Connolly, Yaroslav O Halchenko, Bryan R Conroy, M Ida Gobbini, Michael Hanke, and Peter J Ramadge. A common, high-dimensional model of the representational space in human ventral temporal cortex. *Neuron*, 72(2):404–416, 2011.
- [15] Kentaro Yamada, Yoichi Miyawaki, and Yukiyasu Kamitani. Inter-subject neural code converter for visual image representation. *NeuroImage*, 113:289–297, 2015.
- [16] Matthew Brett, Ingrid S Johnsrude, and Adrian M Owen. The problem of functional localization in the human brain. *Nature reviews neuroscience*, 3(3):243–249, 2002.
- [17] J Swaroop Guntupalli, Michael Hanke, Yaroslav O Halchenko, Andrew C Connolly, Peter J Ramadge, and James V Haxby. A model of representational spaces in human cortex. *Cerebral cortex*, 26(6):2919–2934, 2016.
- [18] Po-Hsuan Cameron Chen, Janice Chen, Yaara Yeshurun, Uri Hasson, James Haxby, and Peter J Ramadge. A reduced-dimension fmri shared response model. *Advances in neural information processing systems*, 28, 2015.
- [19] Hans P Op de Beeck. Against hyperacuity in brain reading: spatial smoothing does not hurt multivariate fmri analyses? *Neuroimage*, 49(3):1943–1948, 2010.
- [20] Alexander Lorbert and Peter J Ramadge. Kernel hyperalignment. *Advances in Neural Information Processing Systems*, 25, 2012.
- [21] Hao Xu, Alexander Lorbert, Peter J Ramadge, J Swaroop Guntupalli, and James V Haxby. Regularized hyperalignment of multi-set fmri data. In *2012 IEEE statistical signal processing workshop (SSP)*, pages 229–232. IEEE, 2012.
- [22] James V Haxby, J Swaroop Guntupalli, Samuel A Nastase, and Ma Feilong. Hyperalignment: Modeling shared information encoded in idiosyncratic cortical topographies. *elife*, 9:e56601, 2020.
- [23] Tomoyasu Horikawa and Yukiyasu Kamitani. Generic decoding of seen and imagined objects using hierarchical visual features. *Nature Communications*, 8(1):1–15, 5 2017.
- [24] Emily J Allen, Ghislain St-Yves, Yihan Wu, Jesse L Breedlove, Jacob S Prince, Logan T Dowdle, Matthias Nau, Brad Caron, Franco Pestilli, Ian Charest, et al. A massive 7t fmri dataset to bridge cognitive neuroscience and artificial intelligence. *Nature neuroscience*, 25(1):116–126, 2022.
- [25] Daniel LK Yamins, Ha Hong, Charles F Cadieu, Ethan A Solomon, Darren Seibert, and James J DiCarlo. Performance-optimized hierarchical models predict neural responses in higher visual cortex. *Proceedings of the national academy of sciences*, 111(23):8619–8624, 2014.
- [26] Michael Eickenberg, Alexandre Gramfort, Gaël Varoquaux, and Bertrand Thirion. Seeing it all: Convolutional network layers map the function of the human visual system. *NeuroImage*, 152:184–194, 2017.
- [27] Haiguang Wen, Junxing Shi, Yizhen Zhang, Kun-Han Lu, Jiayue Cao, and Zhongming Liu. Neural encoding and decoding with deep learning for dynamic natural vision. *Cerebral cortex*, 28(12):4136–4160, 2018.
- [28] Haiguang Wen, Junxing Shi, Wei Chen, and Zhongming Liu. Deep residual network predicts cortical representation and organization of visual features for rapid categorization. *Scientific reports*, 8(1):3752, 2018.

- [29] Roman Belyi, Guy Gaziv, Assaf Hoogi, Francesca Strappini, Tal Golan, and Michal Irani. From voxels to pixels and back: Self-supervision in natural-image reconstruction from fmri. *Advances in Neural Information Processing Systems*, 32, 2019.
- [30] Guy Gaziv, Roman Belyi, Niv Granot, Assaf Hoogi, Francesca Strappini, Tal Golan, and Michal Irani. Self-supervised natural image reconstruction and large-scale semantic classification from brain activity. *NeuroImage*, 254:119121, 2022.
- [31] Kendrick N Kay, Thomas Naselaris, Ryan J Prenger, and Jack L Gallant. Identifying natural images from human brain activity. *Nature*, 452(7185):352–355, 2008.
- [32] Guohua Shen, Tomoyasu Horikawa, Kei Majima, and Yukiyasu Kamitani. Deep image reconstruction from human brain activity. *PLoS computational biology*, 15(1):e1006633, 2019.
- [33] Thomas Naselaris, Ryan J Prenger, Kendrick N Kay, Michael Oliver, and Jack L Gallant. Bayesian reconstruction of natural images from human brain activity. *Neuron*, 63(6):902–915, 2009.
- [34] Kendrick N Kay, Thomas Naselaris, and Jack L Gallant. fmri of human visual areas in response to natural images. *CRCNS. org*, 2011.
- [35] Tomoyasu Horikawa and Yukiyasu Kamitani. Attentionally modulated subjective images reconstructed from brain activity. *bioRxiv*, 2020.
- [36] Jun Kai Ho, Tomoyasu Horikawa, Kei Majima, and Yukiyasu Kamitani. Inter-individual deep image reconstruction. *bioRxiv*, pages 2021–12, 2022.
- [37] Paul S Scotti, Atmadeep Banerjee, Jimmie Goode, Stepan Shabalin, Alex Nguyen, Ethan Cohen, Aidan J Dempster, Nathalie Verlinde, Elad Yundler, David Weisberg, et al. Reconstructing the mind’s eye: fmri-to-image with contrastive learning and diffusion priors. *arXiv preprint arXiv:2305.18274*, 2023.
- [38] Jia Deng, Wei Dong, Richard Socher, Li-Jia Li, Kai Li, and Li Fei-Fei. ImageNet: A large-scale hierarchical image database. In *2009 IEEE Conference on Computer Vision and Pattern Recognition*, pages 248–255. IEEE, 6 2009.
- [39] Tsung-Yi Lin, Michael Maire, Serge J. Belongie, Lubomir D. Bourdev, Ross B. Girshick, James Hays, Pietro Perona, Deva Ramanan, Piotr Doll’ar, and C. Lawrence Zitnick. Microsoft COCO: common objects in context. *CoRR*, abs/1405.0312, 2014.